Water Uptake, Distribution, and Mobility in Amorphous Poly(D,L-Lactide) by Molecular Dynamics Simulation

TIAN-XIANG XIANG, BRADLEY D. ANDERSON

Department of Pharmaceutical Sciences, College of Pharmacy, University of Kentucky, Lexington, Kentucky 40536

Received 27 September 2013; revised 23 December 2013; accepted 24 December 2013

Published online 22 January 2014 in Wiley Online Library (wileyonlinelibrary.com). DOI 10.1002/jps.23855

ABSTRACT: An explicit all-atom computational model for amorphous poly(lactide) (PLA) was developed. Molecular dynamics simulations of PLA glasses were conducted to explore various molecular interactions and predict certain physical properties. The density of a newly formed PLA glass aged for 100 ns at 298 K was 1.23 g/cm^3, close to the experimental range (1.24–1.25 g/cm^3). The glass transition temperature (T_g = 364 K) was higher than experimental values because of the fast cooling rate (0.03 K/ps) in the simulation. The solubility parameter (20.6 MPa$^{1/2}$) compared favorably to the literature. The water sorption isotherm obtained by relating the excess chemical potential of water in PLA to the Henry's law constant for water sorption was close to the experiment. At 0.6% (w/w), water molecules localize next to polar ester groups in PLA because of hydrogen bonding. Local mobility in PLA as characterized by the atomic fluctuation was sharply reduced near the T_g, decreasing further with aging at 298 K. The non-Einsteinian diffusion of water was found to correlate with the rotational β-relaxation of PLA C=O groups at 298 K. A relaxation–diffusion coupling model proposed recently by the authors gave a diffusion coefficient (1.3×10^{-8} cm^2/s at 298 K) which is comparable to reported experimental values. © 2014 Wiley Periodicals, Inc. and the American Pharmacists Association J Pharm Sci 103:2759–2771, 2014

Keywords: amorphous; diffusion; water sorption; glass; glass transition; materials science; mobility; molecular dynamics; polymers; solid-state stability

INTRODUCTION

The molecular events governing water uptake into pharmaceutical solids and the influence of moisture uptake on solid-state formulation properties have been recurring themes in the pharmaceutical literature for several decades. Current understanding in these areas rests to a significant extent on the pioneering research of Zografi and coworkers.[1–9] During a period when the development of high-energy amorphous drug dispersions has emerged as a key enabling technology to enhance oral bioavailability of poorly soluble drugs,[10] Zografi's explorations of the mechanisms of water uptake into amorphous solids and the role of water as a plasticizer to influence both physical and chemical stabilities have provided key insights. One of these was the notion that because of the disordered state of amorphous solids, "it is possible for water to dissolve in the solid," thus setting the stage for an increased appreciation within the pharmaceutical sciences community for the profound effects of water on such properties as the glass transition temperature (T_g) and changes in molecular mobility that may ultimately influence the degree of physical and chemical reactivity.[1] Because of the important impact of water on polymer properties and the stability of amorphous drug formulations, a significant body of work from Zografi and his coworkers also focused on the underlying water–polymer interactions.[2,3,7,8]

Molecular dynamics (MD) simulations are becoming increasingly useful for exploring molecular interactions that govern drug solubility, moisture uptake, and mobility in amorphous formulations. Ultimately, predictions from MD simulations may facilitate excipient selection and formulation design, activities that today require extensive and often costly trial-and-error experiments.[11–17] Work from our own laboratory has demonstrated the utility of MD simulations for understanding the nature of interactions that govern the dissolution of water in amorphous solids and the influence of water content on water cluster formation[11,12]; water mobility[11,12]; and the influence of drug–polymer interactions, drug concentration, and water content on phase miscibility and drug solubility in amorphous formulations.[16,17]

Recent years have witnessed a growing interest in the field of biodegradable polymers and, consequently, in computational activities to explore various molecular properties of biodegradable polymers.[18–21] Poly(lactide) (PLA) and its copolymers are among the most widely used synthetic biodegradable polymers for drug encapsulation and delivery with several products for controlled release of proteins or peptides on the market.[22–24] Biodegradable polymers such as PLA and its copolymers are also useful for applications in biotechnology (e.g., medical devices, implants, and tissue engineering), packaging, and other areas.[24–27]

Despite growing interest, explicit all-atom MD studies of such fundamental properties as water solubility, diffusivity, and distribution in PLA polymers are still lacking. This study is intended to develop a realistic molecular representation of an amorphous PLA solid that can then be useful for predicting PLA properties of pharmaceutical relevance such as the solubility parameter and structural relaxation parameters. In particular, using molecular structures and trajectories obtained from MD simulations, the moisture sorption isotherm of water in PLA and the heterogeneous distribution and diffusion coefficient of water in simulated PLA matrices have been characterized. These properties are of general importance in determining the stability of amorphous drug formulations and in this sense

Correspondence to: Bradley D. Anderson (Telephone: +859-218-6536; Fax: +859-257-2489; E-mail: bande2@email.uky.edu)

Journal of Pharmaceutical Sciences, Vol. 103, 2759–2771 (2014)

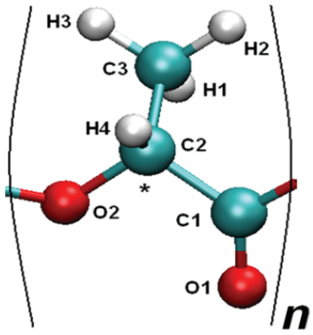

Figure 1. Chemical structure of the PLA-repeating unit with atomic numbering (* indicates the position of the chiral center).

such simulations may provide useful insights applicable to a variety of pharmaceutically relevant amorphous solids.

COMPUTATIONAL METHODS

Poly(lactide) structures were built using Amber/xLeap (University of California, San Francisco, California). The force-field parameters associated with different atomic types were assigned by analogy with existing parameters in the Amber database (ff03). Each PLA chain comprised 100 covalently linked lactic acid monomers and two –OH end groups for a total molecular weight (MW) of 7224 Da, which falls within the wide MW range (2000–200,000) of commercial PLA products.[28,29] The backbone carbon C2 in each PLA monomer (cf., Fig. 1) is a chiral center. Adjacent lactic acid pairs, or dyads, along a PLA chain are in either an (L, L), (D, L), (L, D), or (D, D) conformation. The PLA model in this study was built with D- and L-lactic acid (50%:50%). The dyad sequences were determined by assigning to each chiral center a random number between 0.0 and 1.0 with a D (L) conformation being chosen when the random number fell within 0.0–0.50 (0.50–1.0). Partial charges for PLA repeat units (cf., Table 1) were determined by using a lactic acid trimer with two –OH terminal groups as a model molecule. The energy-minimized trimer was further optimized with HF/6–31G^{**} using Gaussian 09 followed by an electrostatic potential (ESP) calculation at the level of B3LYP/ccpVTZ30 along with the IEF-PCM model using methyl acetate as a model solvent.[30–32] The ESPs obtained were then fitted with the RESP method[33,34] to yield the partial charges in the lactic acid trimer and those for the central repeat unit were fine-tuned to maintain charge neutrality.

Table 1. Atomic Names, Types, and Partial Charges for PLA-Repeat Unit

Atomic Name	Atomic Type	Charge/e
C1	C	0.7597
C2	CT	0.3091
C3	CT	– 0.3892
H1	HC	0.1227
H2	HC	0.1227
H3	HC	0.1227
H4	H1	0.0588
O1	O	– 0.5643
O2	OS	– 0.5423

Using the molecular model developed for PLA polymer along with the TIP3P model for water molecules,[35] assemblies containing five PLA chains and 12 water molecules were constructed. The water content (0.6%, w/w) chosen is comparable to the experimental water content of 0%–1% (w/w) based on moisture sorption isotherm data obtained within a relative humidity range of 0%–100%.[36,37] These assemblies were first constructed in an enlarged cubic box to avoid bad contacts and then energy minimized to further eliminate bad contacts followed by equilibration with periodic boundary conditions for approximately 10 ns at 600 K. The equilibrated assemblies were then subjected to dynamic runs during which the systems were cooled to a final temperature of 200 K at a rate of 0.03 K/ps. After the completion of the cooling process, a microstructure acquired at a certain temperature (298–500 K) was used as a starting configuration for a dynamic run (4–100 ns) at 298, 400, or 500 K, during which system trajectories were acquired at 0.01 ns intervals for subsequent analyses. In addition, an assembly of 1879 water molecules was also simulated at 298 K to compare the interaction energy of water in amorphous PLA solid and pure liquid water.

The energy minimizations and dynamic runs were performed in Sander 12, wherein Newton's equations of motion were evolved using the Verlet leapfrog algorithm[38] with a time step of 1 fs and a dielectric constant of 1.0. The simulated assemblies were coupled to an external thermal bath to maintain a nearly constant temperature and pressure (1 bar).[39] Electrostatic interactions were calculated using the Particle Mesh Ewald method[40] with a cutoff of 10 Å. The SHAKE algorithm was used to constrain all covalent bonds involving hydrogen. The ptraj/Amber program, the molecular graphics program VMD 1.8.7,[41] and other computer programs developed in-house were utilized to numerically calculate various structural and dynamic properties and visually analyze the simulated assemblies. Calculations were performed on a Lipscomb HPC cluster (Dell Inc, Round Rock, TX.) rated at greater than 40 teraflops at the High Performance Computing Complex, University of Kentucky, and PCs in the authors' laboratory.

The excess chemical potential (μ^{exc}) for water (w) in simulated PLA polymers was calculated by the method of Widom[42] as expressed below:

$$\mu^{exc}(w|PLA) = -RT \ln < \exp(-\Delta E_{v\rightarrow PLA}/RT) > \qquad (1)$$

where R is the gas constant, $\Delta E_{v\rightarrow PLA}$ is the change in the potential energy of a simulated PLA assembly as a result of inserting a water molecule from a vapor phase into it, and the angled brackets represent an ensemble average over all the randomly inserted water molecules. As only a very small number of insertions (<0.3%) gave favorable interaction energies, the calculation efficiency was improved by first determining those insertions where the minimum distance between the inserted water molecule and any atom in the PLA matrix exceeded 2.45 Å followed by calculation of $\Delta E_{v\rightarrow PLA}$ for these effective insertions. The statistical convergence of the particle insertion method was tested by varying the number of particle insertions over $N_{ins} = 10^5$–10^8.

The cohesive energy density, CED = E_v/V, of the simulated PLA assembly was calculated where E_v and V are the energy of vaporization and volume of the polymer, respectively. From the CED, the solubility parameter (δ) could be determined

according to:

$$\delta = \sqrt{\text{CED}} \tag{2}$$

By analogy with the Hansen method,[43] δ was decomposed into electrostatic (δ_{ele}) and van der Waals components (δ_{vdW}),

$$\delta^2 = \delta_{ele}^2 + \delta_{vdW}^2 = \frac{E_{ele}}{V} + \frac{E_{vdW}}{V} \tag{3}$$

where the electrostatic component δ_{ele} includes contributions from both polar and hydrogen bonding interactions. E_v, E_{ele}, and E_{vdW} in Eqs. (2) and (3) were calculated, respectively, from the differences of the total potential energies, electrostatic interaction energies, and van der Waals interaction energies for all molecules in the simulated assemblies and in a vacuum when they were infinitely separated from each other.

RESULTS AND DISCUSSION

Physical Properties of PLA Glass

The partial atomic charges for the ester groups in the present PLA model calculated using the combined methods of B3LYP/ccpVTZ30, IEFPCM, and RESP were 0.760 (C1), −0.564 (O1), and −0.542 (O2), respectively (Table 1). Using the 6–31G^* basis set and various partitioning schemes, Koller et al.[44] studied the atomic charge distributions in a series of methyl esters (methyl formate, methyl acetate, and methyl propionate) in the absence of a solvent model and found the charges for the carbonyl carbon and oxygen to be in a narrow range of 0.76–0.98 and −0.58 to −0.62, respectively, whereas that for the ether oxygen was −0.37 to −0.55. Aside from differences in chemical structure between PLA monomers and the model esters described above, different quantum-mechanical (QM) methods and solvent models were also employed. For example, Koller et al.[44] found that the inclusion of a reaction field to account for the medium effect lowered the energy of the ether oxygen–water complex perhaps because of a more pronounced polarization effect of the medium on the charge partitioning between the carbonyl and ether oxygen atoms. Klauda et al.[45] conducted full AM1 level calculations for methyl acetate and other model ester molecules, which served as the basis for optimization of the charges and other nonbonded parameters in more complex phospholipids, and obtained a set of partial charges for these three atoms of 0.48 (C1), −0.43 (O1), and −0.36 (O2). The QM method used in the present study is consistent with the Amber force field as described by Duan et al.[30] The partial charges for the terminal groups in PLA were judiciously assigned based on the present *ab initio* calculations and previous calculations of the same groups in other molecular species and the assumption of overall charge neutrality for each PLA polymer. For the terminal hydrogen atom covalently bonded to the –OCH– group in a PLA repeat unit to form an –OH group, the partial charge was set at a value of 0.36. A similar value (0.40) was assigned to the hydrogen atom for the hydroxyl group in heparin.[46] To maintain charge neutrality, the terminal –OH group attached to the terminal carbonyl group in a PLA repeat unit to form a –COOH group was assigned charge values of (−0.74 and 0.38). These are comparable to those obtained for acetic acid (−0.66 and 0.45) using the same *ab initio* method.

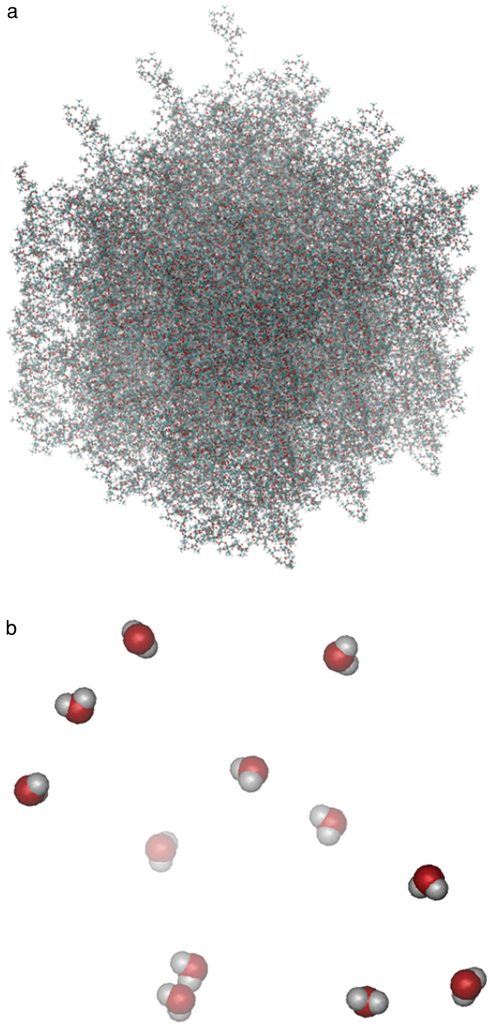

Figure 2. Images of a simulated structure for: (a) a newly formed amorphous PLA solid at 298 K (central and ±x, ±y, ±z image cells) and (b) the corresponding water distribution in the same assembly.

Because of the chiral nature of lactic acid (cf., Fig. 1), PLA polymers can exist in many different conformations differing in isomeric L/D content and sequence. The ratio of L- to D-lactic acid units influences the physical properties of PLA polymers.[47,48] Those having the greatest diversity in terms of isomeric conformation (i.e., L/D ~50:50) exist as amorphous solids that resist crystallization and may thereby be more suitable as formulation matrices for various pharmaceutical applications.[47] Thus, in this study, model PLA polymers comprising randomly distributed 50% L-lactic acid and 50% D-lactic acid units were built and used to construct PLA assemblies.

Once a PLA assembly was built and equilibrated at 600 K, the PLA melt was cooled to 200 K to form a glass at a cooling rate of 0.03 K/ps. Figure 2a shows a representative microstructure of a newly formed PLA glass at 298 K. The amorphous PLA exhibited an apparent T_g, as shown by the plot of density versus temperature (cf., Fig. 3) obtained during the cooling dynamic run. As noted in Figure 3, changes of density versus temperature were steeper at higher temperature, becoming more flat as temperature was lowered below 350 K. The T_g was determined from the intersection of straight-line fits above and below T_g.[13]

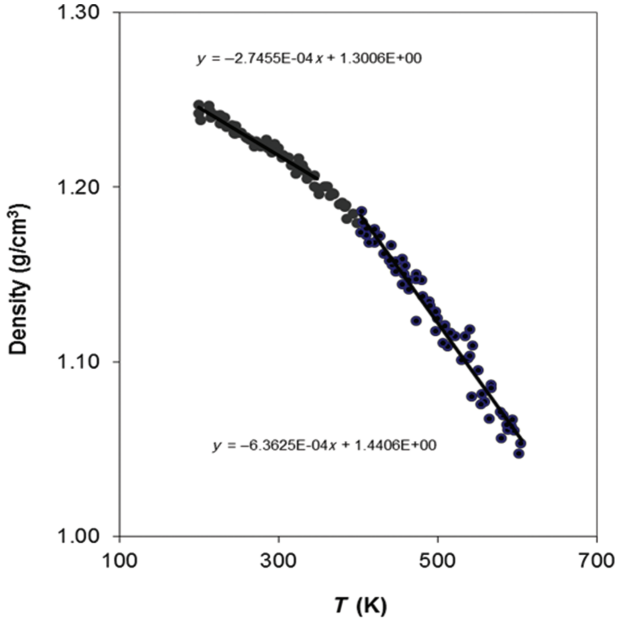

Figure 3. Density vs. temperature phase diagram for the simulated PLA assembly acquired during a cooling process from 600 to 200 K at a rate of 0.03 K/ps.

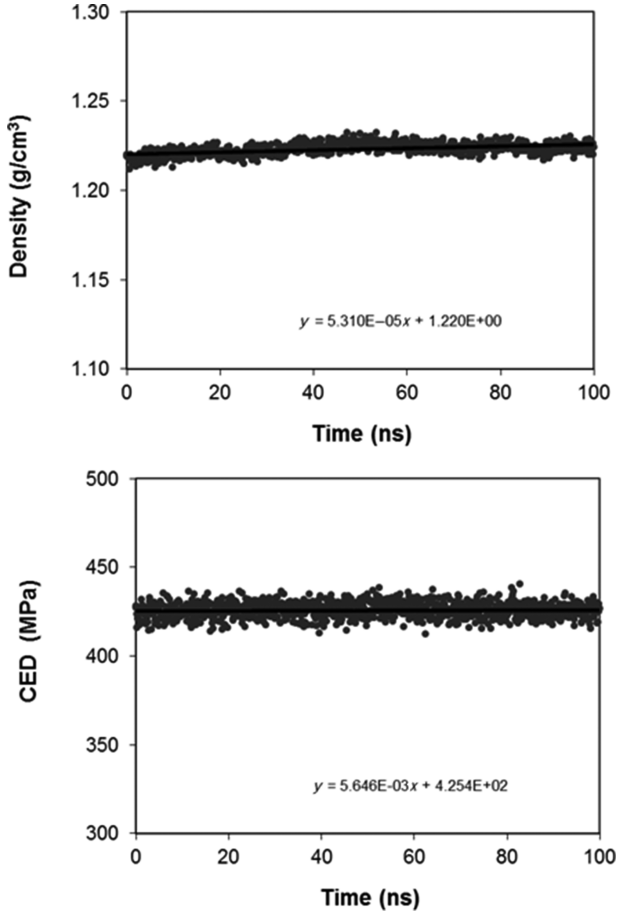

Figure 4. Aging evolution of the density and cohesive energy at 298 K following the formation of the amorphous PLA glass.

The T_g value so obtained, 364 K, is close to those obtained in recent MD simulations by Zhang et al.[49] (361–392 K depending on polymer chain length). An experimental T_g of 52°C (325 K) was reported by Siparsky et al.[48] for PLA (L–D = 50:50). Thus, the T_g values calculated in this and other MD studies[49] are tens of degree higher than the experimental value. The fast cooling rate applied in the MD simulations is considered to be primarily responsible for this discrepancy. This effect has been well established by previous experimental and computational studies.[11,50,51]

Polymer density (d_{PLA}) or the associated property of mean-free volume is one of the most important physical properties characterizing the degree of molecular packing, which in turn determines the resistance to drug diffusion. It is thus highly desirable to develop a molecular model that reproduces reasonably well the density of a real PLA glass, even though glasses are nonequilibrium states having structural properties that may vary with the preparation method and storage history. Unfortunately, relatively few density values for PLA have been reported in the literature, and depending on the percentage of crystallinity, polymer chain length, and distribution of the D,L isomers, the density could vary over a wide range of 1.21–1.43 g/cm.[3,52] Most recent reports from manufacturers (http://www.absorbables.com/technical/properties.html) list density values between 1.24 and 1.25 g/cm^3 depending on the polymer type and L,D-lactic acid content. In the present MD simulations using the Amber force field (ff03), the density for a newly formed PLA glass at 298 K was 1.22 g/cm^3. The slightly lower density obtained compared with the commonly accepted value of 1.24–1.25 g/cm^3 may be attributed to a shorter chain length for the present PLA model, the equal amounts of D and L isomers that hinders tight packing of the lactic acid repeat units because of the diversity of conformations,[48] and perhaps more importantly, the fast cooling in MD simulations that should create a less energetically stable PLA glass as the polymer chains have little time to rearrange to a more tightly packed structure.

To evaluate the latter contribution and the effects of physical aging on PLA density and other structural and dynamic properties, a newly formed PLA glass was subjected to a prolonged dynamic run (100 ns) at 298 K. Figure 4 shows the evolution of the mass density and CED with aging time. The density increased within the first 50 ns and then leveled off at longer simulation times. At the end of the simulation (100 ns), the density approached a value of 1.23 g/cm^3, which is closer to the experimental density of 1.24–1.25 g/cm^3. Over the same time interval, the CED increased by 0.13% over 100 ns, suggesting the formation of a slightly more stable PLA glass.

Water Sorption into PLA Polymer

The tendency for water to absorb into PLA was first characterized by its excess chemical potential in the simulated PLA polymer calculated by the method of Widom.[42] This method has been successfully employed to predict solubility of water in various polymers and lipid membranes.[53–56] The statistical convergence of the calculation was evaluated by changing the number of insertions (N_{ins} = 10^5–10^8) and calculating and comparing the corresponding errors as presented in Figure 5. The SD (1/2 of the error bar height in Fig. 5) decreased with the number

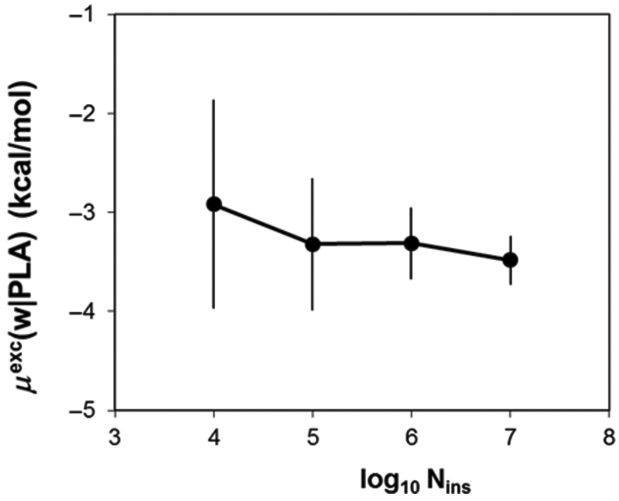

Figure 5. Variation of the excess chemical potential for water in a newly formed PLA glass at 298 K with the number of water molecules inserted.

of insertions with the excess chemical potential approaching $\mu^{\mathrm{exc}}(\mathrm{w}\,|\,\mathrm{PLA}) = -3.4 \pm 0.2$ kcal/mol at $N_{\mathrm{ins}} = 10^7$.

The excess chemical potential of a solute is intrinsically related to its solubility in the material of interest at a given vapor pressure. The theoretical representation for generalized solvation processes given by Ben-Naim and Marcus[57] was closely followed in the derivation of this relation. The chemical potential of water in a PLA glass at a given temperature and pressure can be expressed as

$$\mu(\mathrm{w}|\mathrm{PLA}) = \mu^{\mathrm{exc}}(\mathrm{w}|\mathrm{PLA}) + RT\ln\left(\rho_{\mathrm{w/PLA}}\Lambda_{\mathrm{w}}^{3}q_{\mathrm{w/PLA}}^{-1}\right) \qquad (4)$$

where R is the gas constant, $\rho_{\mathrm{w/PLA}}$ is the number density of water in PLA, and Λ_{w} and $q_{\mathrm{w/PLA}}$ are the translational and internal partition functions for water in PLA, respectively. By definition,[57] $\mu^{\mathrm{exc}}(\mathrm{w}\,|\,\mathrm{PLA})$ is the Gibbs free energy change for the introduction of water into PLA with the constraint that its center of mass is at a fixed position and can thus be considered as the excess chemical potential as derived from the particle insertion method of Widom[42] because of the interaction between the inserted water and surrounding PLA polymer molecules. A similar equation can be written for water in the vapor phase (v):

$$\mu(\mathrm{w}|\mathrm{v}) = \mu^{\mathrm{exc}}(\mathrm{w}|\mathrm{v}) + RT\ln\left(\rho_{\mathrm{w/v}}\Lambda_{\mathrm{w}}^{3}q_{\mathrm{w/v}}^{-1}\right) \qquad (5)$$

Consider now that water in the vapor phase is at equilibrium with water molecules absorbed within PLA:

$$\mu(\mathrm{w}|\mathrm{PLA}) = \mu(\mathrm{w}|\mathrm{v}) \qquad (6)$$

Substituting Eqs. (4) and (5) into Eq. (6), we have

$$\mu^{\mathrm{exc}}(\mathrm{w}|\mathrm{PLA}) - \mu^{\mathrm{exc}}(\mathrm{w}|\mathrm{v}) = RT\ln(\rho_{\mathrm{w/v}}q_{\mathrm{w/PLA}}/\rho_{\mathrm{w/PLA}}q_{\mathrm{w/v}}) \qquad (7)$$

For a similar equilibrium process between a saturated water vapor ($\mathrm{v_s}$) and a pure liquid water (l) phase, we have

$$\mu^{\mathrm{exc}}(\mathrm{w}|\mathrm{l}) - \mu^{\mathrm{exc}}(\mathrm{w}|\mathrm{v_s}) = RT\ln(\rho_{\mathrm{w|v_S}}q_{\mathrm{w|l}}/\rho_{\mathrm{w|l}}q_{\mathrm{w|v_s}}) \qquad (8)$$

Combining Eqs. (7) and (8) and assuming that the internal partition function is identical in the condensed PLA and water phases, $q_{\mathrm{w/l}} = q_{\mathrm{w/PLA}}$, we have

$$\begin{aligned}\delta\mu^{\mathrm{exc}} &= \mu^{\mathrm{exc}}(\mathrm{w}|\mathrm{PLA}) - \mu^{\mathrm{exc}}(\mathrm{w}|\mathrm{l}) \\ &= RT\left[\ln(\rho_{\mathrm{w/v}}/\rho_{\mathrm{w/v_s}}) + \ln(\rho_{\mathrm{w/l}}/\rho_{\mathrm{w/PLA}})\right]\end{aligned} \qquad (9)$$

In the limit of low water-vapor pressure where the ideal gas approximation applies, one has the relation $\rho_{\mathrm{w/v}}/\rho_{\mathrm{w/vs}} = P/P_{\mathrm{s}}$, where P and P_{s} are a given water vapor pressure and the saturated water vapor pressure at temperature T, respectively. Transforming the number density of water in PLA and pure liquid water in terms of mass density, one has $\rho_{\mathrm{w/PLA}}/\rho_{\mathrm{w/l}} = \phi_{\mathrm{w}}(d_{\mathrm{PLA}}/d_{\mathrm{l}})$, where ϕ_{w} is the water content by weight (g/g) in PLA and d_{PLA} and d_{l} are the mass densities of PLA polymer and pure liquid water, respectively. Substituting these results into Eq. (9) and assuming low-equilibrium water sorption where Henry's law applies, the sorption isotherm between water content (ϕ_{w}) and the relative humidity ($\mathrm{RH} = P/P_{\mathrm{s}}$) can be expressed as a linear relation:

$$\phi_{\mathrm{w}} = K(P/P_{\mathrm{s}}) \qquad (10)$$

where the Henry's constant, K, can be approximated as:

$$K = e^{-(\mu^{\mathrm{exc}}(\mathrm{w}|\mathrm{PLA}) - \mu^{\mathrm{exc}}(\mathrm{w}|\mathrm{l}))/RT}(d_{\mathrm{l}}/d_{\mathrm{PLA}}) \qquad (11)$$

Consequently, the water sorption isotherm is uniquely determined by the constant K. The excess chemical potential of water ($\mu^{\mathrm{exc}}(\mathrm{w}\,|\,\mathrm{l}) = -5.74$ kcal/mol) and density ($d_{\mathrm{l}} = 1.0$ g/cm^3) in pure liquid water have been reported in literature based on available experimental results.[58] Thus, the water sorption isotherm in PLA can be calculated from $\mu^{\mathrm{exc}}(\mathrm{w}\,|\,\mathrm{PLA})$ and d_{PLA} results obtained from the present MD simulations. The results are presented in Figure 6 along with those obtained experimentally[37] for comparison. The agreement is within the statistical uncertainty and both the computational and experimental results indicate a low level of water sorption in PLA (<2%, w/w, water content in the range of 0%–100% relative humidity), which can

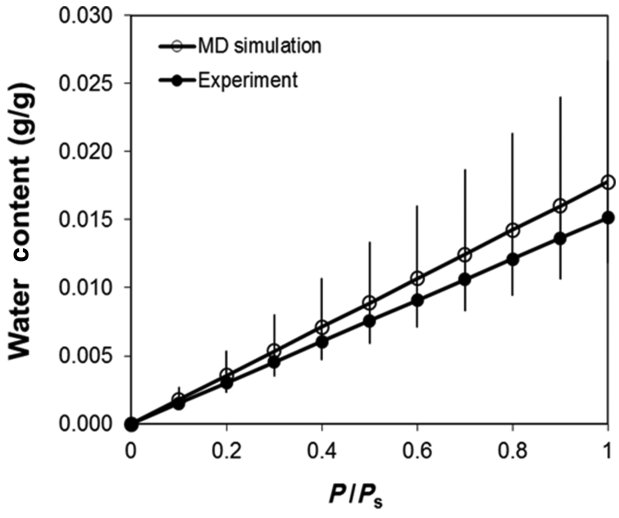

Figure 6. Comparison of water sorption isotherms in PLA at 298 K obtained by the present MD simulation and experiment.[37]

be ascribed to generally weaker interactions between water and PLA compared with those in pure liquid water, as discussed in the next section.

Water Distribution in PLA Polymer

For PLA and related biodegradable polymers, MD simulations enable one to avoid hydrolytic reactions that complicate interpretation of experimental water solubility/diffusivity data generated in PLA polymers. Water molecules absorbed within the PLA matrix may not be distributed uniformly because of the varying interaction strengths with different atoms in PLA as well as with each other. Heterogeneous distribution of water in PLA has been suggested to play an important role in determining the rate of hydrolysis of PLA, whereas other abnormal experimental phenomena have also been attributed to the distribution of water.[36,48,59] For example, water clustering has been proposed as a possible reason for the fact that the observed heat of water solvation (−9.6 kcal/mol) in certain PLA polymers is close to that (−10.5 kcal/mol) for pure liquid water.[48] In addition, Siparsky et al.[48] and Yoon et al.[60] observed that the solubility and diffusivity of water in PLA polymers are independent of the crystallinity content. This observation has been used as an argument for the existence of water clusters in PLA glasses, though it does not rule out the possibility that water clusters may form more readily in crystalline and semicrystalline PLA polymers wherein water may be sequestered from the tightly packed crystalline domains. Other experimental studies have shown scaling between the percent crystallinity and water solubility.[61]

A snapshot of water molecules in a newly formed PLA glass at 298 K is shown in Figure 2b. It indicates that most water molecules are not associated with each other in the simulated PLA glass at 0.6% water content by weight. Snapshots of water molecules near the end of an aging process (100 ns) were also inspected visually and no significant change of water distribution was found, even though water molecules had traversed a distance of approximately 10 Å over 100 ns (see the section on *Molecular Mobility in PLA Glass* and *Water Diffusivity in PLA Glass*). These results appear to contradict previous suggestions of water cluster formation in PLA as mentioned by Cairncross et al.[36] The lack of water clusters observed may, however, stem from the amorphous nature of PLA (L–D = 50:50) where the PLA polymers are less densely packed.

Other evidence supporting a lack of water clustering in amorphous D,L-PLA polymers is the finding of a lower heat of water sorption than that in bulk water.[48] Thus, a comparison of the interaction energy of water in amorphous PLA solid and pure liquid water would be of interest because electrostatic contributions such as hydrogen bonding are so important to the overall interaction energy for water molecules. Average interaction energies for water in the simulated PLA glass and bulk water at 298 K were calculated to be −12.3 and −22.3 kcal/mol, respectively. The much weaker interaction for water in the amorphous PLA solid supports the experimentally observed higher heat of water sorption in PLA polymers containing a sizable amount of both D- and L-lactic acids,[48] and suggests once again a lack of widespread water clustering in amorphous D,L-PLA solid.

Hydrolysis in PLA polymers has been hypothesized to depend on the tendency of water molecules to bind to hydrolytic reaction sites near the ester groups in PLA. For example, Schmitt et al.[59] identified two types of water: unbound water and water

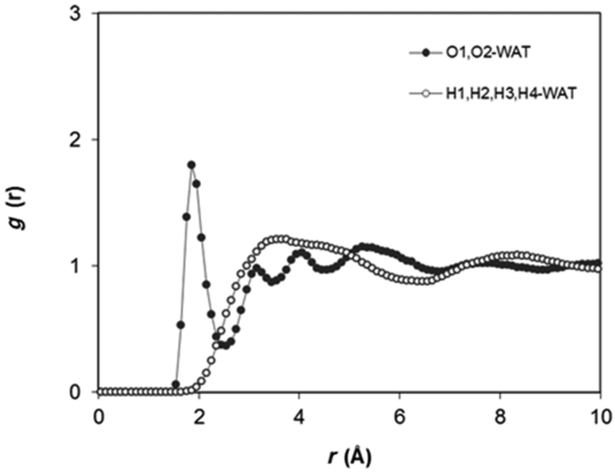

Figure 7. Radial distribution functions, $g(r)$, between the hydrogen atoms in water molecules and the oxygen (solid circles) and hydrogen atoms (open circles) in PLA in the simulated PLA glass at 298 K.

that is hydrogen bonded to the ester groups. Figure 7 shows the radial distribution function, $g(r)$, between the hydrogen atoms (HW) in water molecules and the oxygen (O) and hydrogen atoms (H) in the simulated PLA glass. The absence of a strong peak for $g(r)$ and a value of $g(r)$ less than 1 at a distance of less than 3 Å between HW and nonpolar hydrogen atoms in the methyl/methylene groups on PLA suggest that water molecules stay away from the nonpolar hydrogen atoms on PLA chains. In contrast, a strong peak at 1.85 Å for $g(r)$ between water HW and the oxygen atoms in the ester groups on PLA indicates preferable binding of water molecules with polar ester groups in the PLA polymers.

Interactions between water and the ester groups in PLA were further evaluated by their tendency to form hydrogen bonds (HBs), which were identified by a proton-acceptor distance of less than 3.5 Å and an angle between the proton-donor bond and the line connecting the donor and acceptor atoms greater than 120°. Indeed, both bound and unbound water molecules were found in the PLA glass, though most of the water molecules were hydrogen bonded to the carbonyl oxygen atoms in PLA with probabilities for water to form 0, 1, 2, and 3 HBs with the ester groups in PLA of 0.17, 0.33, 0.50, and 0.0, respectively. Approximately half of the water molecules were involved in two HBs with PLA, forming a bridge between two neighboring lactic acid units, whereas about a third of the water molecules formed a single HB with a lactic acid unit. Representative configurations of these water HBs are illustrated in Figure 8. The existence of these distinctive water states, namely, (1) nonbonded water or water molecules weakly bound to the ether oxygen atom in PLA, (2) water molecules forming a single HB to a carbonyl oxygen atom in PLA, and (3) doubly hydrogen-bonded water molecules, has also been observed in recent time-resolved ATR–FTIR studies of PLA and PLA–PEG diblock copolymer films by Jin et al.[62,63] Interestingly, water molecules are bound mostly to the carbonyl oxygen atoms on PLA (p ~0.93 vs. 0.06 for the ether oxygen atoms), even though both the carbonyl and ether oxygen atoms have similar partial charges (O1: −0.564 and O2: −0.542). An inspection of the HB geometries between water and PLA in Figure 9 reveals that the surface accessible area available for water to HB to the

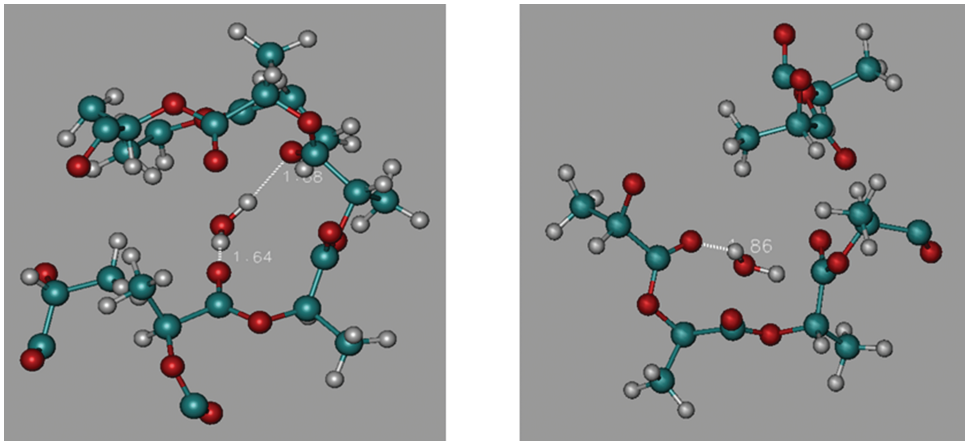

Figure 8. Representative hydrogen bonding configurations for a water molecule with neighboring PLA ester groups in the simulated PLA glass at 298 K: left, two HBs; and right, single HB.

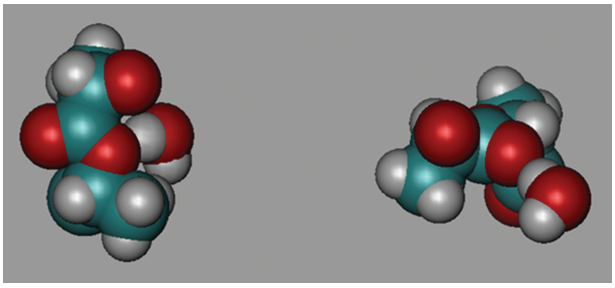

Figure 9. Space-filling representation of hydrogen bonding between a water molecule and a carbonyl (right) and ether group (left) in the simulated PLA glass. For clarity, only two adjacent lactic acid units in the simulated PLA along with the hydrogen bonded water molecule are displayed.

ether oxygen atom is markedly limited compared with the carbonyl oxygen atom. Thus, it is this steric hindrance rather than the atomic charges that effectively excludes the ether oxygen atoms as hydration sites.[44] This is consistent with the experimental evidence that favors water binding at the carbonyl atom in some simple organic compounds.[44] No water molecules were hydrogen bonded to the terminal –OH groups perhaps because of the scarcity of these –OH groups compared with the rich abundance of ester groups in PLA. These results appear to be in contrast with the suggestion by Cairncross et al.[36] based on their sorption experimental observations that moisture sorption is controlled by hydrophilic end groups in PLA.[36,48]

Solubility Parameter for Amorphous PLA Solid

In the pharmaceutical industry, drug–excipient miscibility is commonly predicted by the solubility parameter method developed on the basis of Hildebrand's solubility theory,[14,64–66] even though recent studies have exposed this method's limitations for accurately predicting miscibility.[17,67] Differences in solubility parameters, $\Delta\delta$, of less than 7.0 $MPa^{1/2}$ between materials have been considered as a criterion for compatible systems, whereas those with $\Delta\delta$ of greater than 10.0 $MPa^{1/2}$ are considered likely to be immiscible with each other.[64] The solubility parameter for simulated PLA glass and its polar and nonpolar components were calculated from the present MD simulations and compared with some common materials in Table 2.

Table 2. Solubility Parameter $(MPa)^{1/2}$ for Simulated PLA Compared with Those for Some Other Common Materials

Substance	δ	δ_{vdW}	δ_{ele}
PLA	20.6[a]	13.6[a]	15.0[a]
n-Hexane	14.9[b]	14.9[c]	0
Methyl acetate	18.7[c]	15.5[c]	10.5[c]
Glucose	38.9[c]	–	–
Water	47.9[b]	15.6[c]	45.2[c]
Poly(ethylene)	16.2[d]	–	–
PEG-4000	20.8[e]	–	–
IMC	25.5[f]	20.6[f]	14.4[f]

[a] Present MD study.
[b] Ref. 68.
[c] Ref. 69.
[d] Ref. 70.
[e] Ref. 71.
[f] Ref. 17.

The shortcomings of the solubility parameter method may be attributed in part to the difficulty in determining solubility parameters experimentally. The reliability of various group contribution methods to estimate solubility parameters is still uncertain, especially in dealing with amorphous polymeric solids, as the group-contribution databases are usually based on experimental results for simple organic compounds. They ignore such factors as the internal conformational constraints pervasive in polymeric materials and changes in internal energy and density that accompany physical aging for thermodynamically nonequilibrium glassy solids.

Because of the widespread interest in using PLA polymers, the solubility parameter for PLA (δ_{PLA}) has been extensively studied. The results reported thus far in the literature vary over a range of 19–23 $MPa^{1/2}$, partly because of the use of different PLA species and determination methods. Earlier, using Fedor's[72] group contribution method, Shogren[61] found a δ_{PLA} value of 22.7 $MPa^{1/2}$. Karst and Yang[19] calculated the solubility parameter for PLA using various group contribution methods, obtaining an average δ_{PLA} of 20.2 $MPa^{1/2}$. Using similar group contribution methods, Liu et al.[66] obtained δ_{PLA} of 23.3 $MPa^{1/2}$. Schenderlein et al.[73] performed both the turbidity titration experiments and group contribution calculations for D,L-PLA and various poly(D,L-lactide-co-glycolide) copolymers and obtained

the solubility parameters of $\delta_{PLA} = 19.8$ and 21.7 $MPa^{1/2}$, respectively. On the basis of swelling experiments, Tsuji and Sumida[74] estimated a solubility parameter for L-PLA in a range of 19–20.5 $MPa^{1/2}$. In a dissipative particle dynamics study of L-PLA, Wang et al.[21] obtained δ_{PLA} of 20.5 $MPa^{1/2}$. In this explicit all-atom MD simulation, we obtained a δ_{PLA} of 20.6 $MPa^{1/2}$ for PLA (L–D = 50:50). This result is near the lower end of previously reported δ_{PLA} values. It is comparable to that (18.7 $MPa^{1/2}$) found for methyl acetate, a compound structurally similar to PLA monomers. Compared with the widely used group contribution methods, the MD calculation has the advantage of taking into full account the effects of varying polymer conformations and the thermodynamic (glassy) state on δ_{PLA}.

To further understand the interaction mechanisms that exert a strong influence on the overall solubility parameter, the van der Waals and electrostatic components of the solubility parameter were also calculated ($\delta_{vdW} = 13.6$ and $\delta_{ele} = 15.0$ $MPa^{1/2}$). Both van der Waals and electrostatic interactions have comparable contributions to the overall solubility parameter. A similar result (9.7 vs. 11.8 $MPa^{1/2}$) was found by Liu et al.[66] based on a group-contribution method, though both components are markedly smaller than our results. In contrast, Wang et al.[21] reported a much smaller contribution from electrostatic interactions (6.4 vs. 19.5 $MPa^{1/2}$ for δ_{vdW}). It is unclear whether this has something to do with their use of a cruder coarse-grain molecular model in their computation.

Molecular Mobility in PLA Glasses

Molecular mobility is one of the most important properties governing drug stability and rates of drug release from amorphous solid dispersion-based drug delivery systems.[22] One indicator of local molecular mobility in the simulated amorphous PLA solid is the atomic fluctuation within a given time interval, which was calculated in this study from the root-mean-squared distance of all atoms in the PLA assembly from their average positions in adjacent snapshots separated by 1 ns. The results during the cooling (12 ns from 600 to 200 K) and aging processes (100 ns at 298 K) are presented in Figure 10. The atomic fluctuation was sharply reduced during the cooling process from 2.1 Å/ns at 600 K to 0.34 Å /ns at 298 K with the turning point appearing to be somewhere above the T_g (387 K) as determined from the density-T phase diagram in Figure 3. This is not surprising as, according to the mode-coupling theory,[75] molecular motion effectively ceases near a temperature (T_c) above T_g. During the aging process, the system mobility continues to decrease, albeit at a much slower pace. This is also consistent with the observed decrease in system density (cf., Fig. 4) and corresponding free volume that governs molecular mobility.

Because of the nonequilibrium nature of glassy polymers leading to thermodynamic properties that depend on preparation and storage history, those relaxation processes that reflect residual molecular mobility become extremely important in understanding the polymer stability. Although active investigation of structural relaxation in L-PLA and related copolymer networks has been undertaken,[76–79] much less has been carried out for L,D-PLA.[80] Structural relaxation can be traced back to cooperative and noncooperative motions of various polymer segments, among which the carbonyl groups (C=O) in PLA with their strong dipole moments may be largely responsible for dielectric relaxation spectroscopy commonly used to characterize structural relaxation in PLA. Because of the involvement of

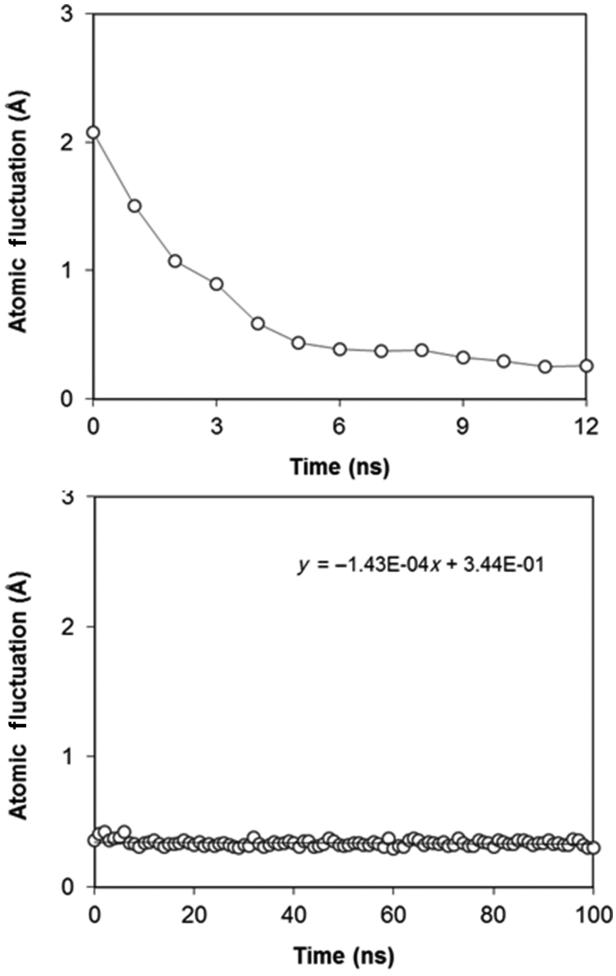

Figure 10. Atomic fluctuation in the PLA assembly during the cooling (upper panel) and aging processes (bottom panel).

PLA carbonyl groups in HB formation with water, their rotational relaxation should be intimately related to water diffusivity in PLA glasses. Thus, the reorientation correlation function for the carbonyl groups in the simulated PLA glasses was calculated. The results averaged over all the carbonyl groups in the simulated PLA are presented in Figure 11. At 298 K, after a sharp decay within 1 ps that corresponds to free rotation within a confining cavity, two distinctive decays, a fast one between 0.001 and 1 ns and a slow one at more than 1 ns, are evident. To further understand the dynamic mechanisms for structural relaxation, molecular trajectories for the PLA polymer were also acquired at 400 and 500 K. These results are also shown in Figure 11. In contrast to the relaxation profiles below T_g, only one decaying component exists above T_g, suggesting a merging of the two relaxation processes that were detected below T_g. Similar behaviors have been observed in other polymeric materials.[81,82] The fast and slow decaying components probably originate from local (β-) and cooperative (α-) relaxation processes. In terms of mode-coupling theory, β-relaxation results mostly from temporary localization of diffusing polymer segments because of dynamic arrest (caging).[13] The dynamic processes for these two types of structural relaxation are often fitted to the Kohlrausch–Williams–Watts (KWW) stretched

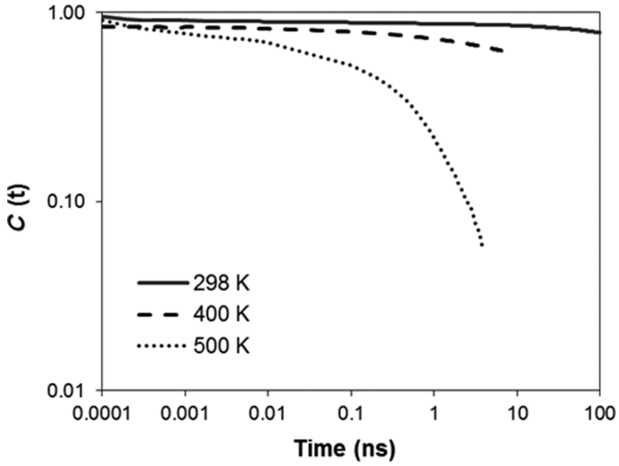

Figure 11. Averaged correlation functions for rotational relaxation of carbonyl groups (C=O) in the simulated PLA assemblies.

exponential function[83–85]:

$$C_{\mathrm{KWW}} = C_0 \exp[-(t/\tau)^{\beta}] \tag{12}$$

where τ and β are the central relaxation time and the stretching parameter, respectively. β varies between 0 and 1 and measures the broadness of the dynamic distribution. Thus, the correlation functions in Figure 11 were fitted with one (at $T > T_g$) or two (at $T < T_g$) KWW functions. The fitted β value for the α-process varied in a narrow range of 0.48–0.51 over 298–500 K, which is close to the β value of 0.51 for the α-process at 353 K in mostly amorphous PLA.[79] A much smaller β (0.23) was obtained for the fast decay at 298 K, suggesting a much broader distribution of relaxation modes for the β-process. Above T_g, the calculated relaxation times (τ) were 0.6 ns at 500 K and 67 ns at 400 K. A broad-band dielectric relaxation experiment by Mijovic and Sy[77] gave τ = ~0.3 ns at 452 K in amorphous L-PLA. At a sub-T_g temperature of 298 K, the τ values found from the simulations for the two decaying components were 0.2 ns and 84 μs, which are markedly smaller than those (~40 ns and >1 s) found for β- and α-processes in L-PLA glasses[77] or related L-PLA homopolymer networks.[78] The correlation time, 84 μs, for the slow decay is also smaller than that (0.03 s) found for the α-process in PLA (L/D = 80/20) at 323 K.[80] We note that the slow decay at 298 K is far from complete and τ and β are highly correlated with a small change in β leading to a large change in τ. Thus, the results at 298 K can only be considered as a rough estimation and an accurate determination would require a simulation time longer than more than 10 μs. Other factors such as differences in polymer L/D content, chain length, measurement subject, and preparative method (an extremely fast cooling rate is typical for simulations) may also contribute to the discrepancies between simulation and experiment results.

Water Diffusivity in PLA Glass

Molecular mobility in the simulated PLA polymers was further evaluated by monitoring the diffusivity of water. One of the major challenges to commercialization of bio-based polymers for some applications is their inferior moisture barrier properties compared with conventional synthetic polymers. Shogren[61] found that typical values of water vapor permeability (WVTR) for biodegradable polyesters (20–300 g/m^2 per day at 25°C) are much higher than those for polymers that display good barrier properties such as polyethylene (~1 g/m^2 per day). Furthermore, because PLA is hydrolytically degradable, the degree of water penetration during manufacturing, shipping, storage, and end use of PLA products determines the physicochemical stability of the polymer.[36] Thus, understanding moisture transport, which is usually characterized in terms of the solubility and diffusion coefficient of water in the polymer of interest, is extremely important. The experimental determination of water diffusivity in PLA is particularly challenging because it is difficult to separate the diffusion process from hydrolytic degradation, and as a result, accurate measurement of water transport requires analyzing the simultaneous diffusion/reaction processes.[48]

According to the Einstein relation,

$$D = \lim_{t\to\infty} D_t = \lim_{t\to\infty} \frac{< |r(t_0 + t) - r(t_0)|^2 >}{6t} \tag{13}$$

where the angled brackets represent an ensemble average over all molecules of the same kind and time origins (t_0), solute diffusivity can be evaluated by monitoring the mean-squared displacement (MSD) over a sufficiently long time (t). The results for water molecules in the simulated PLA glass at 298 and 400 K are presented in the left panels of Figure 12 as log–log plots. The MSD plots as a whole failed to exhibit linear profiles with slopes of one as predicted from the Einstein relation. The degree of this non-Einsteinian behavior at different time intervals was assessed here by the slope (n) of a linear fit, or the following power law:

$$< |r(t_0 + t) - r(t_0)|^2 \propto t^n \tag{14}$$

As shown in Figure 12, at 298 K, n varied from 0.34 at short times (<1 ns) to 0.62 within the latest time interval (up to 100 ns). Thus, water diffusion became less anomalous with time, though it remained non-Einsteinian at 100 ns. Similar non-Einsteinian behaviors have also been observed in another MD simulation of water diffusion in PLA,[86] though it was performed over a much shorter time scale (1 ns). The non-Einsteinian behaviors are greatly diminished above T_g as the n values approach one (0.95) at 400 K even within a shorter time frame of 10 ns.

To further understand the impact of non-Einsteinian behavior on the determination of water diffusivity, the diffusion results were analyzed in terms of the apparent diffusivity (D_t) as defined in Eq. (13) and shown in the right panels of Figure 12. If Einsteinian diffusion holds, D_t should be a constant independent of time. The decay of D_t over time shown in Figure 12 is thus reminiscent of the structural relaxation shown in Figure 11. In a recent MD study,[16] non-Einsteinian diffusion in glassy solids was attributed to structural relaxation and a relaxation-coupling diffusion model was formulated on the basis of this hypothesis:

$$D_t = D + C \exp[-(t/\tau)^{\beta}] \tag{15}$$

Interestingly, as shown in Figure 12, the use of the same KWW parameters (τ = 0.21 ns and β = 0.23) for the β-relaxation process involving PLA C=O rotations at 298 K gives a very

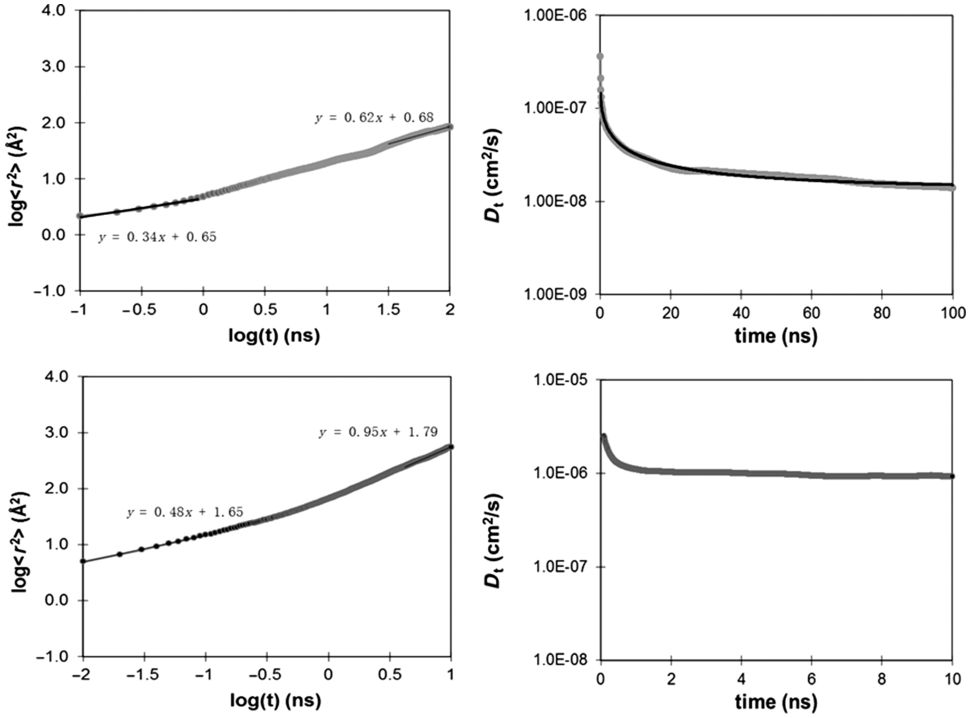

Figure 12. Left panel: log–log plots of the MSDs, $<r^2>$, for water molecules in the simulated PLA glass at 298 K (top) and 400 K (bottom). Right panel: apparent diffusivity (D_t) profiles for water in the PLA glass formed at 298 K (top) and 400 K (bottom) versus time. The solid lines are the least-squares fits.

good description of the diffusivity profile for water at the same sub-T_g temperature. Thus, an important conclusion emerges from the present study that it is the β-process that is largely responsible for the observed non-Einsteinian diffusion behavior of water. This suggests that the apparent diffusivity profile for water could be predicted by using certain dynamic parameters derived from structural relaxation experiments. Further study is needed to understand whether this is specific to water molecules as they bind strongly with the carbonyl groups in PLA or more broadly applicable. Correlations between non-Einsteinian diffusion and β-relaxation have also been found for diffusion of polymer chain segments in other glassy polymers (e.g., 1,4-polybutadiene).[13] Also, though the rotational relaxation for carbonyl groups in PLA at 400 K (cf., Fig. 11) is far from complete in 10 ns, the D_t profile (cf., Fig. 12) has reached a plateau value within 1 ns (i.e., <10% change in D_t from 1 to 10 ns), and the use of the KWW parameters obtained from a fit of the rotational relaxation profile of C=O groups in PLA at 400 K fails to appropriately describe the diffusivity profile of water at the same temperature. These results suggest that this relaxation process, designated as the α-process above T_g, has little role in causing the observed non-Einsteinian diffusion behavior observed for water.

A regression analysis of the results in Figure 12 where only the D and C parameters in Eq. (15) were adjustable gave an extrapolated diffusion coefficient of 1.3×10^{-8} cm^2/s at 298 K. Previous studies of water diffusivity in PLA gave results varying over several orders of magnitude (10^{-6}–10^{-9} cm^2/s) under comparable conditions (i.e., water content ≤2%, w/w; temperature ~20–50°C). Using an MD simulation method, Entrialgo-Castaño et al.[86] and Gautieri et al.[87] obtained water diffusivities in amorphous L-PLA acid on the order of approximately 3–60 $\times 10^{-7}$ cm^2/s at a water content of 2% (w/w). Experimentally, diffusion coefficients for water molecules in PLA polymers have been measured by various gravimetric and spectroscopic techniques.[60,62] Yoon et al.[60] obtained diffusion coefficients for water in amorphous L-PLA by measuring water sorption kinetics. At 36.5°C and a low humidity (0.024 atm water vapor), the diffusion coefficient was found to be 8.0×10^{-8} cm^2/s. Comparable results (45×10^{-8} cm^2/s at 30°C and 50% RH; 6.7×10^{-8} cm^2/s at 20°C and 90% RH) were obtained for water diffusion in PLA (L–D = 50:50) by Siparsky et al.[48] using a similar gravimetric method. In contrast, a recent spectroscopic study by Jin et al.[62] using the time-resolved ATR–FTIR method gave a much smaller diffusion coefficient for water in amorphous L-PLA (1.4×10^{-9} cm^2/s). Our present simulation result (1.3×10^{-8} cm^2/s) is closer to these reported experimental results than the other MD simulation results reported.[86,87] Apart from the use of different PLA materials, in particular their D–L content, at least part of the discrepancy between the computational and experimental results may stem from differences in temperature and humidity conditions or water content, both of which have been known to strongly affect water diffusivity in amorphous polymers. For example, in the work by Siparsky et al.,[48] the water diffusivity in PLA (L–D = 50:50) increased by nearly one order of magnitude (6.7×10^{-8}–50×10^{-8} cm^2/s) from 20°C to 40°C at 90% RH, and at the same temperature (50°C), water diffusivity increased from 26×10^{-8} to 66×10^{-8} cm^2/s when RH was increased from 50% to 90%. In a separate MD study (to be submitted), we found that water diffusivity in HPMCAS polymer increases by nearly one order of magnitude when the water content is increased from 0.7% (w/w) to 5.7% (w/w). Thus, the higher diffusivity results reported by Entrialgo-Castaño et al.,[86] and Gautieri et al.[87] may be partly attributed to their

use of a higher water content (2%, w/w, vs. 0.6%, w/w, in our present MD study). Discrepancies may also arise from: (1) experimental error (~30%) as reported by Siparsky et al.,[48] (2) hydrolysis reactions in those experiments that deplete water molecules and may have significantly altered physicochemical properties of the underlying PLA polymers, and (3) insufficient equilibration time of the glassy polymers in the experimental measurements, which lends to non-Fickian diffusion as inferred from thickness-dependent diffusion coefficients,[88] and in the present MD simulations and other computational studies.

CONCLUSIONS

An explicit all-atom simulation model for PLA polymer was developed that is capable of approximately reproducing some important physical properties of amorphous PLA solids including material density, water sorption isotherm, and diffusion coefficient, thus verifying its potential utility in designing PLA-based drug delivery systems and in particular for predicting drug–PLA miscibility.[17] The combination of MD simulations, the particle insertion method of Widom,[42] and a theoretical sorption relation elucidated in this work was employed to calculate the water sorption isotherm in PLA. Weak sorption of water in amorphous PLA solids was predicted similar to experimental results. Inspection of molecular structures of the simulated PLA glasses provided further understanding of the distribution of water in PLA polymers that has been difficult to obtain experimentally. In particular, water molecules were found to be mostly separated from each other at a water content of 0.6% by weight, residing more favorably near the ester groups in PLA where they form HBs with carbonyl oxygen atoms. Water diffusion in the glassy PLA was found to exhibit non-Einsteinian behavior over the 100 ns simulation time, which could be modeled satisfactorily by a relaxation–coupling diffusion model using the same correlation time for β-relaxation of C=O groups in PLA. Above T_g, water diffusion became Einsteinian after a short non-Einsteinian decay period (<1 ns), a process that was shown to be distinct from the structural relaxation (α-process) of C=O groups in PLA at the same temperatures. Thus, the present study advances the relaxation–coupling diffusion model[16] by verifying that it is the β and/or related local relaxation processes that are mostly responsible for non-Einsteinian diffusion of water molecules in glassy polymers.

ACKNOWLEDGMENTS

Financial support for this project was obtained from the NSF I/UCRC Center for Pharmaceutical Development. We also thank the University of Kentucky Information Technology Department and Center for Computational Sciences for computing time on the Lipscomb High Performance Computing Cluster and for access to other supercomputing resources.

REFERENCES

1. Ahlneck C, Zografi G. 1990. The molecular basis of moisture effects on the physical and chemical stability of drugs in the solid state. Int J Pharm 62:87–95.
2. Oksanen CA, Zografi G. 1990. The relationship between the glass transition temperature and water vapor absorption by poly(vinylpyrrolidone). Pharm Res 7:654–657.
3. Hancock BC, Zografi G. 1993. The use of solution theories for predicting water vapor absorption by amorphous pharmaceutical solids: A test of the Flory–Huggins and Vrentas models. Pharm Res 10:1262–1267.
4. Hancock BC, Zografi G. 1994. The relationship between the glass transition temperature and the water content of amorphous pharmaceutical solids. Pharm Res 11:471–477.
5. Oksanen CA, Zografi G. 1993. Molecular mobility in mixtures of absorbed water and solid poly(vinylpyrrolidone). Pharm Res 10:791–799.
6. Shalaev EY, Zografi G. 1996. How does residual water affect the solid-state degradation of drugs in the amorphous state? J Pharm Sci 85:1137–1141.
7. Zhang J, Zografi G. 2000. The relationship between "BET"—And "free volume"—Derived parameters for water vapor absorption into amorphous solids. J Pharm Sci 89:1063–1072.
8. Taylor LS, Langkilde FW, Zografi G. 2001. Fourier transform Raman spectroscopic study of the interaction of water vapor with amorphous polymers. J Pharm Sci 90:888–901.
9. Newman AW, Reutzel-Edens SM, Zografi G. 2007. Characterization of the "hygroscopic" properties of active pharmaceutical ingredients. J Pharm Sci 97:1047–1059.
10. Hancock BC, Zografi G. 1997. Characteristics and significance of the amorphous state in pharmaceutical systems. J Pharm Sci 86:1–12.
11. Xiang TX, Anderson BD. 2004. A molecular dynamics simulation of reactant mobility in an amorphous formulation of a peptide in poly(vinylpyrrolidone). J Pharm Sci 93:855–876.
12. Xiang TX, Anderson BD. 2005. Distribution and effect of water content on molecular mobility in poly(vinylpyrrolidone) glasses: A molecular dynamics simulation. Pharm Res 22:1205–1214.
13. Barrat JL, Baschnagel J, Lyulin A. 2010. Molecular dynamics simulations of glassy polymers. Soft Matter 6:3430–3446.
14. Gupta J, Nunes C, Vyas S, Jonnalagadda S. 2011. Prediction of solubility parameters and miscibility of pharmaceutical compounds by molecular dynamics simulations. J Phys Chem B 115:2014–2023.
15. Huynh L, Grant J, Leroux JC, Delmas P, Allen C. 2008. Predicting the solubility of the anti-cancer agent docetaxel in small molecule excipients using computational methods. Pharm Res 25:147–157.
16. Xiang TX, Anderson BD. 2013. Molecular dynamics simulation of amorphous indomethacin. Mol Pharm 10:102–114.
17. Xiang T-X, Anderson BD. 2013. Molecular dynamics simulation of amorphous indomethacin-poly(vinylpyrrolidone) glasses: Solubility and hydrogen bonding interactions. J Pharm Sci 102:876–891.
18. Ahmad S, Johnston BF, Mackay SP, Schatzlein AG, Gellert P, Sengupta D, Uchegbu IF. 2010. In silico modelling of drug–polymer interactions for pharmaceutical formulations. J Roy Soc Interface 7:S423-S433.
19. Karst D, Yang Y. 2005. Using the solubility parameter to explain disperse dye sorption on polylactide. J Appl Polym Sci 96:416–422.
20. Kasimova AO, Pavan GM, Danani A, Mondon K, Cristiani A, Scapozza L, Gurny R, Möller M. 2012. Validation of a novel molecular dynamics simulation approach for lipophilic drug incorporation into polymer micelles. J Phys Chem B 116:4338–4345.
21. Wang YC, Ju SP, Jung T, Wang HH. 2011. Modeling of polyethylene, poly(L-lactide), and CNT composites: A dissipative particle dynamics study. Nanoscale Res Lett 6:433.
22. Fredenberg S, Wahlgren M, Reslow M, Axelsson A. 2011. The mechanisms of drug release in poly(lactic-co-glycolic acid)-based drug delivery systems—A review. Int J Pharm 415:34–52.
23. Hans ML, Lowman AM. 2002. Biodegradable nanoparticles for drug delivery and targeting. Curr Opin Solid St M 6:319–327.
24. Kumari A, Yadav SK, Yadav SC. 2010. Biodegradable polymeric nanoparticles based drug delivery systems. Colloid Surface B 75:1–18.
25. Auras R, Harte B, Selke S. 2004. An overview of polylactides as packaging materials. Macromol Biosci 4:835–864.
26. Auras RA, Lim LT, Selke SEM, Tsuji H, Eds. 2011. Poly(lactic acid): Synthesis, structures, properties, processing, and applications. New York: John Wiley & Sons.

27. Jamshidian M, Tehrany EA, Imran M, Jacquot M, Desobry S. 2010. Poly-lactic acid: Production, applications, nanocomposites, and release studies. Compr Rev Food Sci F 9:552–571.
28. Wichert B, Rohdewald P. 1993. Low molecular weight PLA: A suitable polymer for pulmonary administered microparticles? J Microencapsul 10:195–207.
29. Bodmeier R, Chen H. 1989. Evaluation of biodegradable poly(lactide) pellets prepared by direct compression. J Pharm Sci 78:819–822.
30. Duan YCW, Chowdhury S, Lee MC, Xiong G, Zhang W, Yang R, Cieplak P, Luo R, Lee T, Caldwell J, Wang J, Kollman P. 2003. A point-charge force field for molecular mechanics simulations of proteins based on condensed-phase quantum mechanical calculations. J Comp Chem 24:1999–2012.
31. Miehlich B, Savin A, Stoll H, Preuss H. 1989. Results obtained with the correlation energy density functionals of Becke and Lee, Yang and Parr. Chem Phys Lett 157:200–206.
32. Pomelli CS, Tomasi J, Barone V. 2001. An improved iterative solution to solve the electrostatic problem in the polarizable continuum model. Theor Chem Acc 105:446–451.
33. Bayly CI, Cieplak P, Cornell WD, Kollman PA. 1993. A well-behaved electrostatic potential based method using charge restraints for deriving atomic charges: The RESP model. J Phys Chem 97:10269–10280.
34. Cieplak P, Cornell WD, Bayly C, Kollman PA. 1995. Application of the multimolecule and multiconformational RESP methodology to biopolymers-charge derivation for DNA, RNA, and proteins. J Comp Chem 16(11):1357–1377.
35. Jorgensen WL, Chandrasekhar J, Madura JD, Impey RW, Klein ML. 1982. Comparison of simple potential functions for simulating liquid water. J Chem Phys 79:926–935.
36. Cairncross RA, Becker JG, Ramaswamy S, O'Connor R. 2006. Moisture sorption, transport, and hydrolytic degradation in polylactide. Appl Biochem Biotech 129–132:774–785.
37. Mucha M, Ludwiczak S. 2007. Water sorption by biodegradable chitosan/polylactide composites. Polish Chitin Society, Monograph. XII:41–48.
38. Verlet L. 1967. Computer "experiments" on classical fluids. I. Thermodynamical properties of Lennard–Jones molecules. Phys Rev 159:98–103.
39. Berendsen HJC, Postma JPM, van Gunsteren WF, DiNola A, Haak JR. 1984. Molecular dynamics with coupling to an external bath. J Chem Phys 81(8):3684–3690.
40. Ewald P. 1921. Die Berechnung optischer und elektrostatischer Gitterpotentiale. Ann Phys 64:253–287.
41. Humphrey WA, Dalke Schulten K. 1996. VMD: Visual molecular dynamics. J Mol Graph 14:33–38.
42. Widom B. 1963. Some topics in the theory of fluids. J Chem Phys 39:2808–2812.
43. Hansen CM. 1967. The three dimensional solubility parameter and solvent diffusion coefficient. Copenhagen, Denmark: Technical University of Denmark.
44. Koller J, Merzel F, Hadzi D. 1993. Charge populations of, and water binding at, the oxygen atoms of some simple esters. J Mol Struct 300:233–238.
45. Klauda JB, Venable RM, Freites JA, O'Connor JW, Tobias DJ, Mondragon-Ramirez C, Vorobyov I, MacKerell AD Jr, Pastor RW. 2010. Update of the CHARMM all-atom additive force field for lipids: Validation on six lipid types. J Phys Chem B 114:7830–7843.
46. Becker CF, Guimaraes JA, Verli H. 2005. Molecular dynamics and atomic charge calculations in the study of heparin conformation in aqueous solution. Carbohyd Res 340:1499–1507.
47. Ratner BD. 2004. Biomaterials science: An introduction to materials in medicine. San Diego, California: Elsevier Inc.
48. Siparsky GL, Voorhees KJ, Dorgan JR, Schilling K. 1997. Water transport in polylactic acid (PLA), PLA/polycaprolactone copolymers, and PLA/polyethylene glycol blends. J Env Polym Degrad 5:125–136.
49. Zhang J, Liang Y, Yan J, Lou J. 2007. Study of the molecular weight dependence of glass transition temperature for amorphous poly(L-lactide) by molecular dynamics simulation. Polymer 48:4900–4905.
50. Lyulin AV, Balabaev NK, Michels MAJ. 2003. Molecular-weight and cooling-rate dependence of simulated T_g for amorphous polystyrene. Macromolecules 36:8574–8575.
51. McKenna GB. 1986. Glass formation and glassy behavior. Compr Polym Sci 2:311–362.
52. Polylactic acid. Accessed on 1/8/2014 at: https://en.wikipedia.org/wiki/Polylactic_acid.
53. Canales M, Aradilla D, Alemán C. 2011. Water absorption in polyaniline emeraldine base. Polym Phys 49:1322–1331.
54. Jedlovszky P, Mezei M. 2000. Calculation of the free energy profile of H_2O, O_2, CO, CO_2, NO, and $CHCl_3$ in a lipid bilayer with a cavity insertion variant of the Widom method. J Am Chem Soc 122:5125–5131.
55. Marrink SJ, Berendsen HJC. 1994. Simulation of water transport through a lipid membrane. J Phys Chem 98:4155–4168.
56. Ostwal MM, Sahimi M, Tsotsis TT. 2009. Water harvesting using a conductive polymer. A study by molecular dynamics simulation. Phys Rev E 79:061801.
57. Ben-Naim A, Marcus Y. 1984. Solvation thermodynamics of nonionic solutes. J Chem Phys 81:2016–2027.
58. Hermans J, Patbiaseril A, Anderson A. 1988. Excess free energy of liquids from molecular dynamics simulations. Application to water models. J Am Chem Soc 110:5982–5986.
59. Schmitt EA, Flanagan DR, Lindhardt RJ. 1994. Importance of distinct water environments in the hydrolysis of poly(D,L-lactide-co-glycolide). Macromolecules 27:743.
60. Yoon JS, Jung HW, Kim MN, Park ES. 2000. Diffusion coefficient and equilibrium solubility of water molecules in biodegradable polymers. J Appl Polym Sci 77:1716–1722.
61. Shogren R. 1997. Water vapor permeability of biodegradable polymers. J Env Polym Degrad 5:91–95.
62. Jin Y, Wang W, Su Z. 2011. Spectroscopic study on water diffusion in poly(L-lactide)–poly(ethylene glycol) diblock copolymer film. Macromolecules 44:2132–2139.
63. Jin Y, Wang W, Su Z. 2012. Spectroscopic study on water diffusion in poly(lactic acid) film. Polym Chem 3:2430–2435.
64. Greenhalgh DJ, Williams AC, Timmins P, York PJ. 1999. Solubility parameters as predictors of miscibility in solid dispersions. Pharm Sci 88:1182–1190.
65. Hildebrand JH. 1916. Solubility. J Am Chem Soc 38:1452–1473.
66. Liu H, Finn N, Yates MZ. 2005. Encapsulation and sustained release of a model drug, indomethacin, using CO_2-based microencapsulation. Langmuir 21:379–385.
67. Patel S, Lavasanifar A, Choi P. 2008. Application of molecular dynamics simulation to predict the compatability between water-insoluble drugs and self-associating poly(ethylene oxide)-b-poly(epsilon-caprolactone) block copolymers. Biomacromolecules 9:3014–3023.
68. Burrell H. 1970. Solubility of polymers. Kirk–Othmer encyclopedia of science and technology. 2nd ed. New York: John Wiley & Sons.
69. Barton AFM. 1983. Handbook of solubility parameters and other cohesion parameters. 2nd ed. Boca Raton, Florida: CRC Press.
70. Patrick RL. 1967. Treatise on adhesion and adhesives. New York: Marcel Dekker.
71. Albers J. 2008. Hot-melt extrusion with poorly soluble drugs. Ph.D. Thesis. Dusseldorf, Germany: Heinrich-Heine-Universitat.
72. Fedors RF. 1974. A method for estimating both the solubility parameters and molar volumes of liquids. Polym Eng Sci 14:147–154.
73. Schenderlein S, Luck M, Muller BW. 2004. Partial solubility parameters of poly(D,L-lactide-co-glycolide). Int J Pharm 286:19–26.
74. Tsuji H, Sumida K. 2000. Poly(L-lactide): V. effects of storage in swelling solvents on physical properties and structure of poly(L-lactide). J Appl Polym Sci 79:1582–1589.

75. Götze W. 2009. Complex dynamics of glass-forming liquids: A mode-coupling theory. Oxford, UK: Oxford University Press.
76. Dionısio M, Viciosa MT, Wang Y, Mano JF. 2005. Glass transition dynamics of poly(L-lactic acid) during isothermal crystallisation monitored by real-time dielectric relaxation spectroscopy measurements. Macromol Rapid Commun 26:1423–1427.
77. Mijovic J, Sy JW. 2002. Molecular dynamics during crystallization of poly(L-lactic acid) as studied by broad-band dielectric relaxation spectroscopy. Macromolecules 35:6370–6376.
78. Serra RSI, Ivirico JLE, Duenas JMM, Balado AA, Ribelles JLG, Sanchez MS. 2009. Segmental dynamics in poly(e-caprolactone)/poly(L-lactide) copolymer networks. J Polym Sci B Polym Phys 47:183–193.
79. Shinyama K, Oi T, Fujita S. 2012. Dielectric relaxation phenomena of polylactic acid with β-crystalline chitin. Int J Polym SciVolume 2012: Article ID 389491.
80. Mierzwa M, Floudas G, Dorgan J, Knauss D, Wegner J. 2002. Local and global dynamics of polylactides. J Non-Cryst Solids 207–310:296–303.
81. Bedrov D, Smith GD. 2005. Molecular dynamics simulation study of the α- and β-relaxation processes in a realistic model polymer. Phys Rev E 71:050801.
82. Smith GD, Bedrov D. 2007. Relationship between the α- and β-relaxation processes in amorphous polymers: Insight from atomistic molecular dynamics simulations of 1,4-polybutadiene melts and blends. J Polym Sci B Polym Phys 45:627–643.
83. Kohlrausch R. 1854. Theorie des electrischen Ruckstandes in der Leidner Flasche. Pogg Ann Phys Chem 91:179–214.
84. Williams G, Watts DC. 1970. Non-symmetrical dielectric relaxation behavior arising from a simple empirical decay function. Trans Faraday Soc 66:80–85.
85. Williams G, Watts DC, Dev SB, North AM. 1971. Further considerations of non symmetrical dielectric relaxation behaviour arising from a simple empirical decay function. Trans Faraday Soc 67:1323–1335.
86. Entrialgo-Castaño M, Salvucci AE, Lendlein A, Hofmann D. 2008. An atomistic modeling and quantum mechanical approach to the hydrolytic degradation of aliphatic polyesters. Macromol Sy 269:47–64.
87. Gautieri A, Mezzanzanica A, Motta A, Redealli A, Vesentini A. 2012. Atomistic modeling of water diffusion in hydrolytic biomaterials. J Mol Model 18:1495–1502.
88. Sharp JS, Forrest JA, Jones RAL. 2001. Swelling of poly(D,L-lactide) and polylactide-co-glycolide in humid environments. Macromolecules 34:8752–8760.